

Characterization and Photometric Membership of the Open Cluster NGC 1981

F. F. S. Maia^{*}, W. J. B. Corradi, J. F. C. Santos Jr.

Instituto de Ciências Exatas, UFMG, Av. Antônio Carlos 6627, Belo Horizonte, Brazil

Accepted xxx. Received xxx; in original form 2010 April 09

ABSTRACT

Open clusters belonging to star-forming complexes are the leftovers from the initial stellar generations. The study of these young systems provides constraints to models of star formation and evolution as well as to the properties of the Galactic disc. We aimed at investigating NGC 1981, a young open cluster in the Orion Nebula Region, using near-IR and $BV(RI)_C$ photometric data. We devised a method that accounts for the field contamination and allows to derive photometric membership for the cluster stars. A new cluster centre was determined by Gaussian fittings to the 2-D stellar distribution on the sky, and has been used to obtain the radial stellar density profile and the structural parameters. Mass functions were computed for stars inside the cluster limiting radius and total mass estimated from them. Although more easily distinguished by its grouping of 6 relatively bright stars, an underlying population of faint pre-main sequence stars is evident in the cluster area. We showed that this population is related to the cluster itself rather than to the nearby Orion Nebula cluster. Additionally a fraction of the cluster low mass stars may have been evaporated from the region in its early evolution leading to the present sparse, loose structure. The estimated parameters of NGC 1981 are core radius $R_c = 0.09 \pm 0.04$ pc, limiting radius $R_{\text{lim}} = 1.21 \pm 0.11$ pc, age $t = 5 \pm 1$ Myr, distance modulus $(m - M)_0 = 7.9 \pm 0.1$ (380 ± 17 pc), reddening $E(B - V) = 0.07 \pm 0.03$ and total mass $m = 137 \pm 14 M_\odot$.

Key words: open clusters and associations: general – open clusters and associations: individual: NGC 1981 – galaxy: stellar content – stars: pre-main-sequence

1 INTRODUCTION

The open clusters' fundamental physical parameters are important pieces of information for studies on the formation and evolution of the Galactic disc (e.g., Piatti et al. 1995; Jacobson et al. 2008; Sestito et al. 2008) and as grounding tests for star formation and evolution models (e.g., Landin et al. 1996; D'Antona 2002; Siess et al. 2000). Dias et al. (2002, hereafter DAML02) have summarized the available information on open clusters in a major catalogue which continuously expands. In version 2.10¹ of this catalogue, 1787 open clusters are listed out of which 54 per cent have known distance, age and reddening, 24 per cent have also proper motion and radial velocity and only 10 per cent have metal abundance determined. Kharchenko et al. (2005) have created an open cluster catalogue with uniformly determined parameters, among them cluster radius, core radius and age, by means of an automated computational algorithm

(The Catalogue of Open Cluster Data, COCD)². This catalogue has been used to investigate the local (< 1 kpc) population of star cluster complexes revealing new constraints on the Galaxy's structure and kinematics (Piskunov et al. 2006).

Sky surveys like 2MASS (Skrutskie et al. 2006) produced large amounts of near-IR data and have contributed to the discovery of even more objects. Additionally, several studies have been benefited from 2MASS database by employing near-IR photometric analyses of structural and populational properties of Milky Way star clusters (e.g., Santos Jr. et al. 2005; Pavani & Bica 2007; Bonatto et al. 2006). Because the 2MASS database covers the whole sky, it allows data extraction from spatially unlimited regions. Also, near-IR wavelengths are particularly sensitive to discriminate cluster stars from the contaminating field for young stellar systems (e.g., Santos Jr. et al. 2005).

NGC 1981 (OC1525, C 0532-044) is a young, sparse cluster located $\sim 1^\circ$ North from the Orion Nebula at Galactic

^{*} E-mail: kicage@fisica.ufmg.br

¹ <http://www.astro.iag.usp.br/~wilton>

² <http://www.univie.ac.at/webda/cocd.html>

coordinates $\ell = 208.09^\circ$ and $b = -18.98^\circ$. As noted by Sharpless (1952), *the Orion Nebula seems to be separated from NGC 1981 only as a result of a somewhat nearer obscuring cloud*. NGC 1981 depicts the northern end of Orion's Sword. According to Subramaniam et al. (1995), NGC 1981 and Collinder 70 constitute a possible binary cluster being less than 20 pc apart. The cluster belongs to Gould's Belt, a planar distribution of O and B stars inclined $\sim 20^\circ$ with respect to the Galactic plane (Pöppel 2001, and references therein). In a detailed study of Gould's Belt (Lesh 1968), the brightest stars in the cluster (HD 37016, HD 37017 and HD 37040) had their spectral types determined (B2.5V, B1.5V, B2.5IV, respectively) and photometric distances estimated (all at 494 pc).

Subsequent works emphasized kinematical properties of NGC 1981 stars, among other clusters, aiming at obtaining dynamical and structural characteristics of our Galaxy (e.g., Hron 1987). More recently, Kharchenko et al. (2005) performed an analysis of the cluster as a stellar system deriving reddening $E(B - V) = 0.05$, distance modulus $(V - M_v) = 8.16$ ($d = 400$ pc), $\log t(\text{yr}) = 7.50$, cluster radius $R = 0.25^\circ$ (1.7 pc) and core radius $R_c = 0.13^\circ$ (0.9 pc). We should note, however, that the age estimated by Kharchenko et al. (2005) relies upon a single star, as a consequence of the method applied, which progressively removes stars with low membership probabilities from the CMD by means of an iterative process.

Most studies of the cluster are inserted in more general analyses of the Orion star formation complex. It is part of Orion OB1 association, subgroup c, which is 2 to 6 Myr old and located closer to us (≈ 400 pc) than the younger Orion Nebula by at least 10 pc (Bally 2008). However, such a division in subgroups has been questioned in favour of a continuous star forming event (Muench et al. 2008). Since NGC 1981 bright stars are early B spectral types, a plausible evolutionary sequence would entail supernovae explosions from O-type progenitors causing the compression of the interstellar medium and formation of the present younger populations. On the kinematical side, Dias et al. (2006) derived membership probabilities on the basis of UCAC2 proper motions aided by a statistical method for 158 stars within 15 arcmin of the cluster centre.

Elias et al. (2009) investigated hierarchical star formation in Gould's Belt based on the spatial and kinematical distribution of star clusters, either bound star systems or transient stellar condensations with a mean lifetime of ~ 10 Myr or less. NGC 1981 was classified by them as a bound cluster in view of its age (~ 30 Myr) as determined by Kharchenko et al. (2005). In the present work, we argue that NGC 1981 is indeed younger, as has been shown to be the case for Platais 6 and NGC 2546, which also belong to Gould's Belt (Elias et al. 2009).

Despite the efforts to better understand the astrophysical processes occurring in the Orion Nebula and its surroundings and their connection with Gould's Belt, NGC 1981 have not been given particular attention (except for Kharchenko et al. 2005) and, as a consequence, its parameters can be improved. In this work, we present Johnson-Cousins $BV(RI)_C$ photometric observations carried out at the Observatório do Pico dos Dias (Itajubá, Brazil) along with near-IR photometric data extracted from 2MASS survey to study the open cluster structural properties and stel-

lar content, aiming at a better determination of radius, age, distance, reddening and mass.

This work is structured as follows. Sect. 2 describes the observational data employed. Sect. 3 presents the procedure to obtain the cluster centre, a fundamental step to build a reliable radial density profile, discussed in Sect. 4. Colour-magnitude diagrams are employed in Sect. 5, where a statistical decontamination algorithm is applied to the cluster CMDs, and in Sect. 6, where a comparison of data with isochrones allows a determination of the cluster's astrophysical parameters. In Sect. 7 the radial mass function of the cluster is analysed and in Sect. 8 the stellar density charts used to map the spatial distribution of stars and their frequency in different CMD regions are described. Further discussions and conclusions are given in Sect. 9.

2 DATA

2.1 Near-infrared

Vizier³ was used to extract near-infrared photometric data from 2MASS in circular fields centred on equatorial coordinates (J2000) $\alpha = 05^{\text{h}}35^{\text{m}}09^{\text{s}}$ and $\delta = -04^\circ25'54''$, the cluster centre as taken from DAML02. The data encompasses the point sources within $R < 55$ arcmin, corresponding roughly to four times the estimated visual radius of the cluster. For decontamination purposes, a comparison field was extracted 1° northwest of the cluster, in a region with the same area and similar absorption as deduced from near-infrared (2MASS) and mid-infrared (IRAS) images. This choice was preferred over an annular field extraction centred in the cluster because of the nebulosity associated with NGC 1977 towards the south. Figure 1 shows an image of NGC 1981 and the nearby region from IRAS 60 μm band. The selected comparison field and other objects are also shown.

As photometric quality constraint, the 2MASS extracted data were restricted to unambiguous point sources brighter than specified on the 99 per cent Point Source Catalogue completeness limit (15.8, 15.1 and 14.3 mag for 10- σ at J , H , and K_s , respectively).

2.2 Optical

CCD $BV(RI)_C$ observations were carried out with the 0.6-m (IAG) telescope at the Observatório do Pico dos Dias (Laboratório Nacional de Astrofísica, Itajubá, Brazil) during the night of September 21, 2000. The CCD detector employed was a 1×1 k SItE SI003AB (# 101) configured to yield read-out noise 5.5 e^- and gain $5.0 \text{ e}^- \text{ ADU}^{-1}$. The plate scale was $1.22 \text{ arcsec.pixel}^{-1}$. The images were obtained using a focal reducer to cover a field-of-view of 21×21 arcmin and were taken with a mosaic setup on 6 adjacent positions around the cluster centre in order to cover the full extension of the object. To transform instrumental magnitudes into the standard system, 15 objects from Landolt (1992) standard stars catalogue were also observed on the same night, with 2 standard stars being used for atmospheric extinction correction. Details of the observations are shown in Table 1, where the

³ <http://vizier.u-strasbg.fr/viz-bin/VizieR>

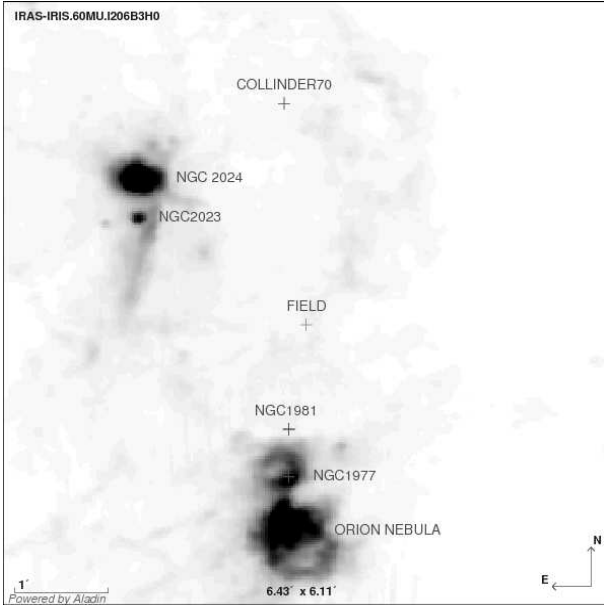


Figure 1. NGC 1981 and the nearby region from IRAS 60 μ m band. Other objects in the area and the selected comparison field are also indicated.

observed fields are listed along with their exposure times, typical seeing values and airmasses.

The data were reduced using the standard IRAF routines for aperture photometry. Besides the standard reduction steps, the 6 adjacent fields have been aligned and recurrent stars were selected according to their distance to the image centre in each filter. Specifically, for every recurrent star, we kept only the measurement of the star closest to the image centre. This choice avoided the *vignetting* effect introduced on the images borders by the focal reducer. The calibration equations used to transform to the standard system were:

$$b = B + b_1 + b_2 X_b + b_3 (B - V) + b_4 (B - V) X_b \quad (1)$$

$$v = V + v_1 + v_2 X_v + v_3 (B - V) + v_4 (B - V) X_v \quad (2)$$

$$r = R + r_1 + r_2 X_r + r_3 (V - R) + r_4 (V - R) X_r \quad (3)$$

$$i = I + i_1 + i_2 X_i + i_3 (V - I) + i_4 (V - I) X_i \quad (4)$$

where B , V , R and I are the standard magnitudes and b , v , r and i are the instrumental magnitudes; X_n is the airmass on each filter. The subscript coefficients $i = 1...4$, were obtained from a 2-pass interactive fitting on each filter with the extinction coefficients (subscripts 2 and 4) being fitted first and then used as constants on a second fit of the zero point and colour terms (subscripts 1 and 3 respectively). The derived coefficients and the RMS deviation of the fittings to the catalogued magnitudes of the standard stars are shown in Table 2.

As photometric quality constraint the employed data set was that restricted to an error less than 0.04 mag, corresponding to the higher deviations found on the calibration fit. This value implies a magnitude limit of approximately 15 mag and leads to an average magnitude uncertainty of 0.05 mag (taking into account the calibration deviation).

The following analysis involving spatial information

Table 1. Observation log for NGC 1981

Cluster/Region	Filter	Exposure (s)	Seeing (")	Airmass
NGC 1981/CE	B	1 15 50	3.4	1.2
	V	1 20	2.5	1.2
	R	1 20	2.4	1.2
	I	1 20	3.9	1.2
NGC 1981/CW	B	1 15 50	3.1	1.1
	V	1 20	2.8	1.1
	R	1 20	2.7	1.1
	I	1 20	3.4	1.1
NGC 1981/NE	B	1 15 50	2.7	1.3
	V	1 20	2.6	1.3
	R	1 20	2.3	1.2
	I	1 20	3.8	1.2
NGC 1981/N	B	1 15 50	3.1	1.1
	V	1 20	2.6	1.1
	R	1 20	2.6	1.1
	I	1 20	3.7	1.1
NGC 1981/NW	B	1 15 50	3.3	1.1
	V	1 20	2.9	1.1
	R	1 20	2.8	1.1
	I	1 20	4.1	1.1
NGC 1981/S	B	1 15 50	3.3	1.1
	V	1 20	2.6	1.1
	R	1 20	2.7	1.1
	I	1 20	3.7	1.1

Table 2. Coefficients and RMS deviation of the calibration fit.

i	B	V	R	I
1	5.79 ± 0.01	5.35 ± 0.01	4.53 ± 0.02	5.05 ± 0.01
2	0.28 ± 0.06	0.17 ± 0.04	0.11 ± 0.04	0.08 ± 0.05
3	-0.19 ± 0.01	-0.20 ± 0.02	-0.18 ± 0.07	-0.11 ± 0.02
4	-0.04 ± 0.04	0.15 ± 0.02	0.19 ± 0.04	0.07 ± 0.03
RMS	0.03	0.02	0.04	0.03

were developed using 2MASS data due to its large extraction area, good astrometry and the poor seeing of the optical data, which was employed mostly for CMD comparisons with the near-IR data.

3 NEW CENTRE DETERMINATION

The sparse aspect of NGC 1981 makes difficult to estimate its centre, which is an essential step before a reasonable radial density profile can be obtained. Catalogued centre values are mainly intended for identification purposes and are generally imprecise. Therefore, we have estimated the centre of NGC 1981 by first selecting a region (see Fig.2) around the coordinates given by DAML02. The search area was limited to the sky around the catalogued centre and did not include stars southward of $\delta = -4.55^\circ$ to avoid the nebosity and contamination from NGC 1977.

Furthermore, the selected region was divided into bins of right ascension and declination and star counts were made

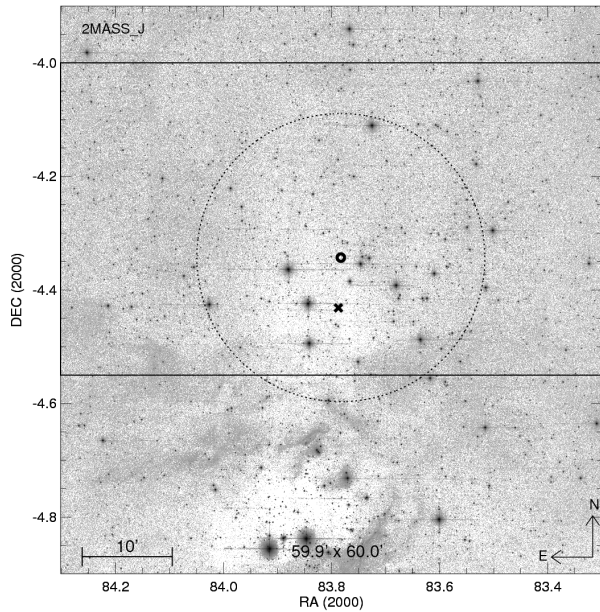


Figure 2. Sky chart of NGC 1981 showing the region used for centre determination (rectangle), the literature centre (cross), the calculated centre (circle) and the data extraction area for the decontamination method (dotted circle).

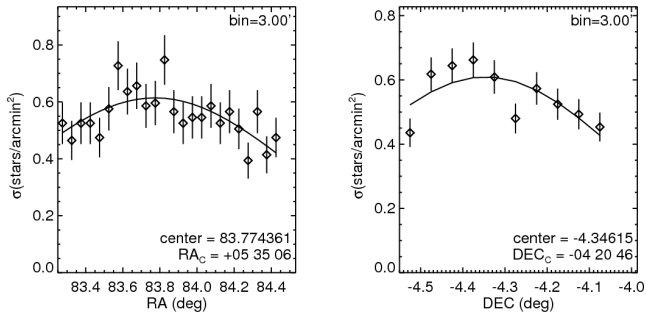


Figure 3. Gaussian fittings for the determination of central coordinates. Bin size on RA and DEC is 3.0 arcmin. Error bars correspond to Poisson statistical errors.

inside them. We used these star counts to build spatial profiles and fitted a Gaussian function to the stars distribution on RA and DEC, adopting the centre of the fitted Gaussian as the cluster centre coordinate. Fig. 3 shows the Gaussian fitting obtained for bin size 3.0 arcmin and the resulting coordinates of the centre.

This procedure was applied to different bin sizes ranging from 0.25 – 4.00 arcmin and the resulting centre coordinates were used to create histograms showing the most recurrent RA and DEC values. We adopted these values as the coordinates of the cluster centre. We also found no trends between the coordinates and the bin size. Figure 4 shows this relationship and the histograms defining the cluster centre.

The adopted coordinates of the cluster centre are $\alpha = 83^{\circ}46'59'' = 5^{\text{h}}35^{\text{m}}08^{\text{s}}$ and $\delta = -04^{\circ}20'35''$. The histograms bin width were chosen based on the standard deviation of the centre coordinates and accounts for an uncertainty of approximately 5 arcsec on α and δ . Fig. 2 shows

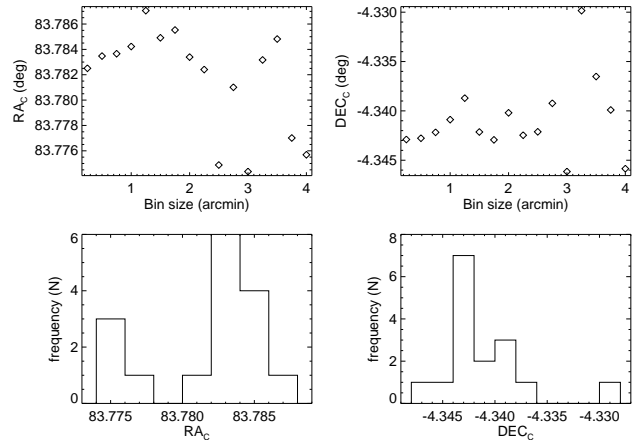


Figure 4. Relation between determined coordinates and the bin size (top). Histograms showing the most recurrent right ascension and declination for the cluster centre (bottom).

that the calculated centre is 5.32 arcmin north and 0.27 arcmin east from the literature centre. The area used for centre determination and the data extraction region for the decontamination method (see Sect. 5) are also shown.

4 RADIAL DENSITY PROFILE

The structural properties of star clusters can be derived by means of a projected density profile such as the radial density profile (RDP). The RDPs of star clusters usually follow an analytical profile and can be described by functions with different parameters related to the cluster structure. These parameters include the tidal radius, core radius, core stellar density and background star density. However, young and sparse open clusters like NGC 1981 usually show little overdensity in comparison to the field making difficult the fitting of analytical functions and so the determination of their structural parameters.

In order to circumvent this problem the density profile was built by superposing RDPs constructed by counting stars inside successive radial rings of fixed width up to 55 arcmin and then dividing by the area of the rings. Ring widths ranged from 0.75 – 2.00 arcmin, with 0.25 arcmin increments. The narrower rings are ideal to probe the core structure of the cluster while the larger ones are better to probe the external regions. This prevents either region of the cluster to be undersampled.

The possible contamination from NGC 1977 stars to the cluster population was investigated with separate radial profiles for the northern and southern region of NGC 1981 using semi-circles based on the central declination ($\delta = -04^{\circ}20'35''$) determined in Sect. 3. Density maps were also built up to the extreme radius of 55 arcmin to allow for the discrimination of subtle stellar density differences between both regions. To obtain a good contrast on the resulting density map an optimal radial bin of 2.5 arcmin was used to calculate the stellar density around each star. Fig. 5 shows the radial profiles of the north (top) and south (bottom) regions and the corresponding density maps (insets).

Although NGC 1977 is about 30 arcmin southwards it

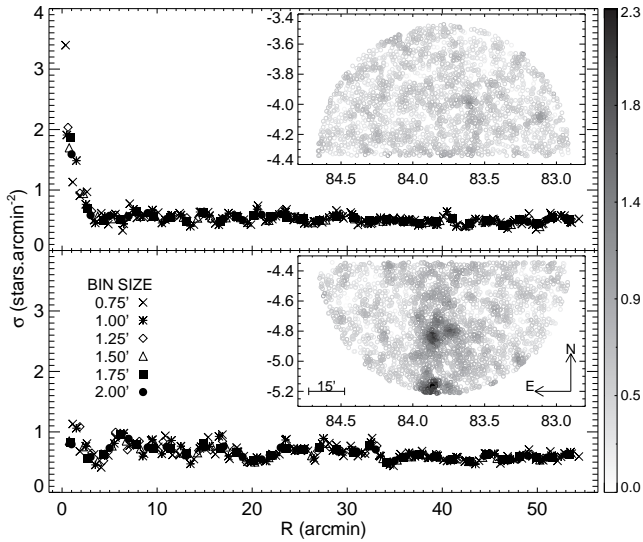


Figure 5. RDP of the north (top) and south (bottom) regions of NGC 1981. Stellar density maps of each region are also shown (insets). Radial ring sizes range from 0.75–2.00 arcmin. Colour-bar on the right represents the stellar density (stars.arcmin^{-2}) on the insets.

can be seen in Fig. 5 that the contribution from its stars clearly affects the density profile of the southern region of NGC 1981. Since it is not possible to tell the boundaries between the two clusters or readily distinguish their stars, we turned to the northern part of the density profile to investigate the structural properties of NGC 1981 by means of analytical density functions.

Trials of King profile fittings were made on the density profile using the two-parameter modified density function introduced by King (1962):

$$f_2(R) = \sigma_{\text{bg}} + \frac{\sigma_0}{1 + (R/R_c)^2}. \quad (5)$$

To provide better convergence the sky level (σ_{bg}) was estimated as the mean of the radial bins inside the range 16–32 arcmin and further subtracted from each radial ring to derive the central density (σ_0) and core radius (R_c) through the 2-parameter King function. The fitting was weighted by the statistical Poissonian errors of the star counts inside each radial ring. Fig. 6 shows the fitting of the 2-parameter function and the sky determination (inset) for the northern region of the cluster with the 1- σ uncertainties of the fittings. The determined parameters R_c and σ_{bg} are also indicated with their associated errors.

The determined structural parameters were central density $\sigma_0 = 2.4 \pm 1.2 \text{ stars.arcmin}^{-2}$, core radius $R_c = 0.83 \pm 0.34 \text{ arcmin}$ and background level $\sigma_{\text{bg}} = 0.54 \pm 0.07 \text{ stars.arcmin}^{-2}$. A cluster limiting radius (R_{lim}) was estimated by visually inspecting the radius where stars from the cluster are completely merged with the background. We found $R_{\text{lim}} = 11 \pm 1 \text{ arcmin}$ for NGC 1981. Using the distance of 380 pc (see Sect. 6), 1 arcmin corresponds to 0.11 pc.

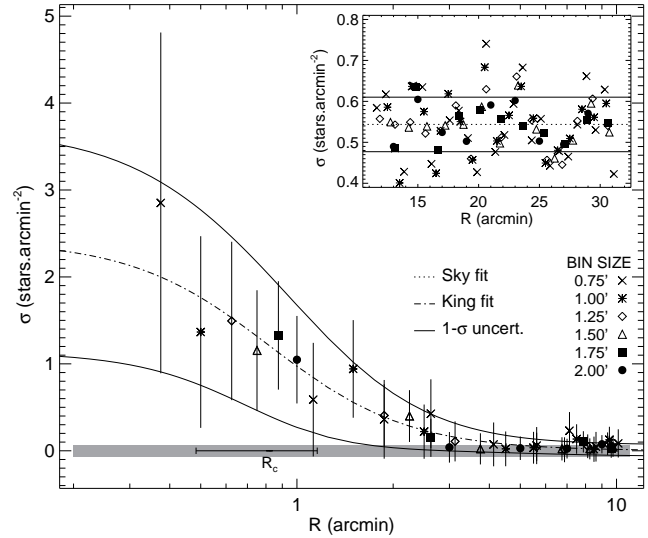


Figure 6. 2-parameter King-profile fittings. Background level was determined beyond 16 arcmin (inset). The determined core radius is indicated. Sky fluctuation is represented by a grey rectangle. Error bars denote 1- σ Poissonian fluctuations.

5 COLOUR-MAGNITUDE DIAGRAMS AND FIELD-STAR DECONTAMINATION

Colour-magnitude diagrams of open clusters usually present well-defined stellar sequences such as the main sequence, turn-off and giant branch that provide essential information on the physical properties of these objects. However, the characterization of open clusters is often hindered by strong reddening and field-star contamination, specially for the objects projected against the Galactic centre or sparsely populated.

The identification of the cluster stars as opposed to the field-star contamination is very important in the study of these objects. Assessing membership using proper motion data is only available for a small subset of the known open clusters, particularly the closest ones. An alternative method for disentangling cluster and field-stars consists of using photometric data by means of statistical comparison of star samples taken from the cluster region and from an offset-field. Our decontamination procedure is one of these methods and was based on the work of Bonatto & Bica (2007).

5.1 Decontamination procedure

A field-star decontamination procedure was carried out by firstly selecting an appropriate comparison field presenting stellar density and reddening similar to the cluster. While circular annular fields circumscribed to the cluster area are appropriated for clusters in dense regions and homogeneous backgrounds, they fail on regions affected by differential reddening or rapidly changing backgrounds. Therefore, an adjacent field with similar reddening was selected for NGC 1981 considering the nebulosity contamination from NGC 1977 in the southern region of the cluster. Regarding the cluster area, the data included stars within the inner 16 arcmin of the determined centre. This central region corresponds to the cluster visual radius, chosen to encompass the brightest B type stars in the field.

We built 3D colour-magnitude diagrams for both cluster and field-stars with J , $J - H$ and $J - K_s$ as axes. These colours provide better discrimination among the clusters sequences on the CMD (Bonatto et al. 2004). The diagrams were divided into small cells of average sizes $\Delta J = 0.6$ mag, $\Delta(J - H) = 0.3$ mag and $\Delta(J - K_s) = 0.3$ mag, corresponding roughly to ten times the average uncertainties in the colours. These cells are small enough to detect local variations of field-star contamination on the various sequences in the CMD, but large enough to accommodate a significant number of stars. The grids in Fig. 8 illustrate these cell sizes.

Initial cluster membership was assigned to cluster stars within each cell based on their overdensity with relation to the field-stars, according to the relation $P = (N_{\text{clu}} - N_{\text{fld}})/N_{\text{clu}}$. Null probability was assigned whenever an excess of field-stars over cluster stars occurred in a given cell. A subset of the original cluster sample was created by removing from each cell on the cluster CMD, the expected number of field-stars as measured in the control field CMD based on their distance to the calculated centre of the cluster. Particularly, each cell on the cluster CMD had the stars most distant from the cluster centre removed and cells without cluster overdensity had all stars inside their limits removed.

In order to account for the initial choice of parameters, we applied the described method for different grid specifications by changing the position and size of the cells in each of the CMD axes. Cell positions were changed by shifting the entire grid one third of the cell size in each direction. Cell sizes were increased and decreased by one third of the average sizes in each of the CMD axes. Considering all possible configurations, 729 different grid sets were used to derive final membership probabilities by taking the average, median and mode of the membership obtained in each configuration for each star. An exclusion index was also created by noting how many times each star was removed from the sample, and then normalizing by the number of grid configurations.

Possible effects of the offset-field selection were investigated by applying the method to 3 additional comparison fields 1° distant from the cluster in different directions northward of the cluster. The average, median and mode of the membership of each star, obtained from the multiple grid configurations, were compared once different offset-fields were employed in the decontamination method. The offset-field selection implied mean deviations of 7 per cent on the average membership, 8 per cent on the median membership and 12 per cent on the mode membership. These values were adopted as the general uncertainty of these statistical indicators. Final membership probabilities were thus assigned to each star by taking the average of the membership from each grid configuration.

The decontaminated sample was obtained by removing stars based on another two complementary criteria. First, stars with average membership value lower than 7 per cent or median membership value lower than 8 per cent were removed. Second, stars with exclusion index larger than 50 per cent were removed. The first criterion ensures the removal of stars that could present null membership, based on the uncertainties of each statistical indicator. The second criterion is based on the exclusion index and decontaminate the cluster sequences by removing the expected field population. The exclusion index threshold (50 per cent) was set to pro-

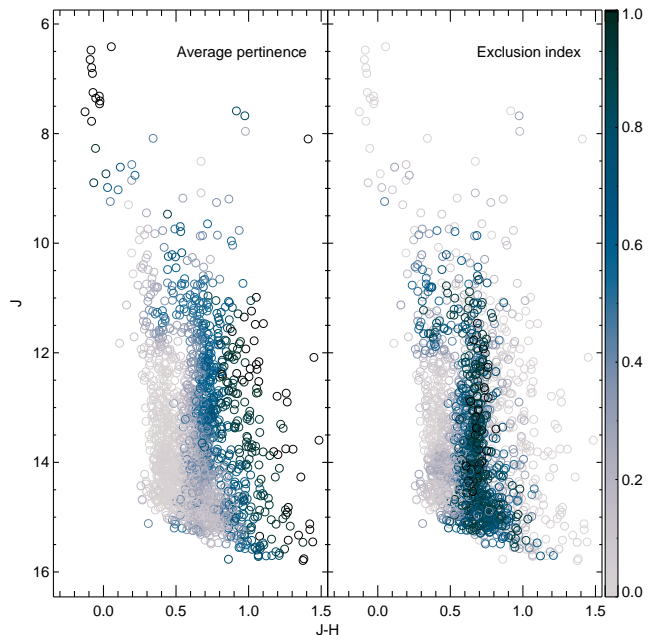


Figure 7. Decontamination domain of the complementary adopted criteria. Note that stars with lower membership probability (left) were removed by the first criterion whereas stars with higher exclusion index (right) were removed by the second criterion. The colourbar indicates both the membership probability (left panel) and the exclusion index (right panel) of stars.

vide the removal of approximately the same number of stars removed by the first criterion.

The adopted criteria complement each other well, acting on different parts of the CMD and presenting very little overlapping of the removed stars. The first criterion removes stars with low membership probability, acting mainly on regions where the cluster and field population are entangled, presenting roughly the same density on the CMD. For NGC 1981 it represents the lower and mid-main sequence/pre-main sequence. For the second criterion, it is worth recalling that stars were removed from each cluster CMD cell according to the counts from the offset-field CMD and on the distance from the cluster centre. Therefore the second criterion clean the cluster sequences from the stars in the outer regions of the cluster and effectively removes from the CMD the stars where field population is dominant. It decontaminates the region of the pre-main sequence stars, mainly for the fainter regions ($J > 10$). Fig. 7 shows the decontamination domain of each criterion.

5.2 Results on NGC 1981

In order to increase the statistical sample and better probe the field population, the procedure was applied on stars within 32 arcmin from the cluster centre and the resulting decontaminated sample, used in the subsequent analysis, was truncated at the visual radius of the cluster (16 arcmin). This truncation was done because the adjacent southern clouds associated to NGC 1977 yield a very reddened population which occupy a well defined region in the CMD (see Sect. 8). The CMD locus of this reddened population does not overimpose that of most cluster stars therefore not

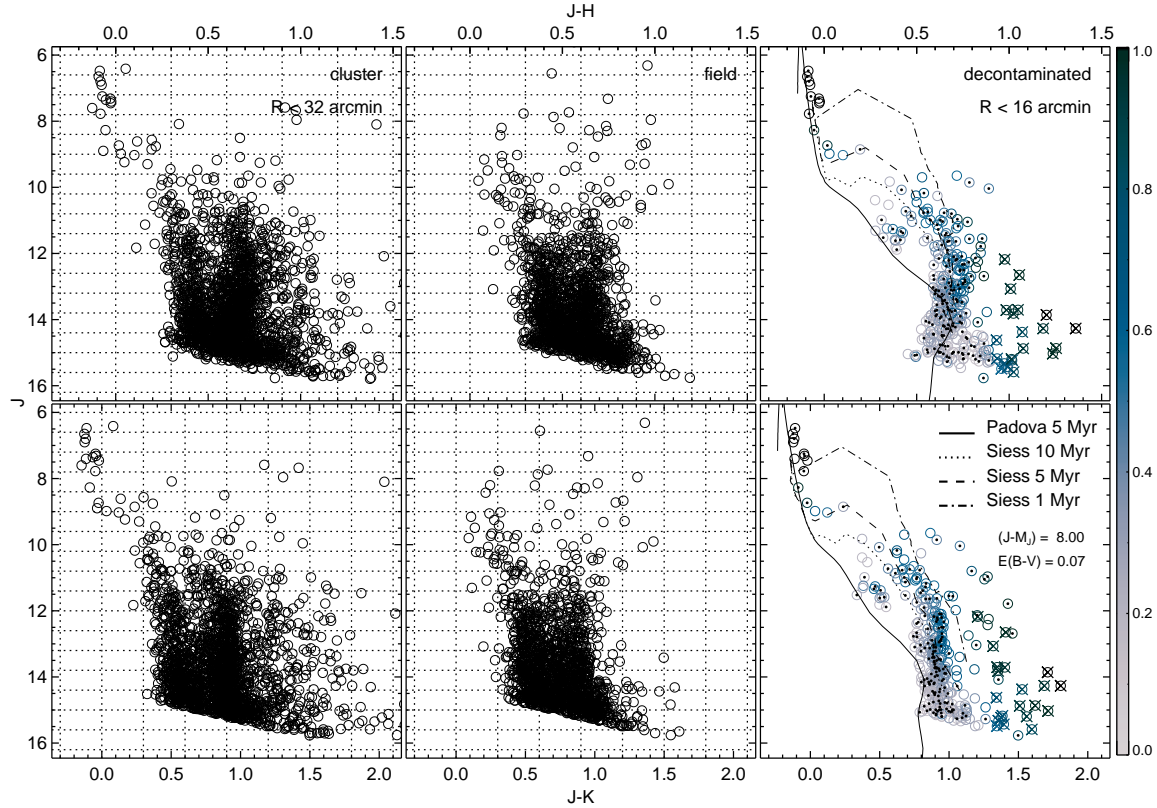


Figure 8. Cluster (left), field (middle) and decontaminated (right) CMDs using $J-H$ (top) and $J-K_s$ (bottom) colours. Very reddened stars, present in the southern region of the cluster were marked with crosses. Stars inside the R_{lim} are marked with dots. The average cell sizes are indicated by dotted grids. MS and PMS isochrone fittings are also shown on the right panels. Colourbar on the right indicate the calculated cluster membership probability.

interfering with the decontamination procedure. However, even inside the visual radius, very reddened stars presenting $J-H > 0.9$ and $J-K_s > 1.2$ appear on the southern region of the cluster (crosses in Fig. 8). They were not properly sampled by the field population and therefore could neither be excluded by the procedure nor present reliable membership probabilities. These stars are likely members of NGC 1977. Fig. 9 shows the sky chart of NGC 1981 up to 16 arcmin, comparing the member and field population. Structural parameters derived in Sect. 4 are also indicated.

The number of stars removed from the contaminated sample do not account for the entire field population because the expected number of field-stars measured on the offset-field is still higher than the number of excluded stars. On average, each criterion removed 45 per cent of the field population while presenting a common exclusion rate of 5 per cent and a total decontamination efficiency of 85 per cent. Most of the exclusion takes place in the crowded areas of the CMD as 95 per cent of the stars excluded belong to the lower main-sequence ($J > 12$).

The choice of the offset-field accounts for an average deviation of 5 per cent in the number of stars left in the decontaminated subsamples (member stars). Moreover the fraction of recurring member stars, independent of the offset-field, is greater than 87 per cent. Fig. 8 compares cluster, field and decontaminated stars in the $J \times J-H$ and $J \times J-K_s$ diagrams.

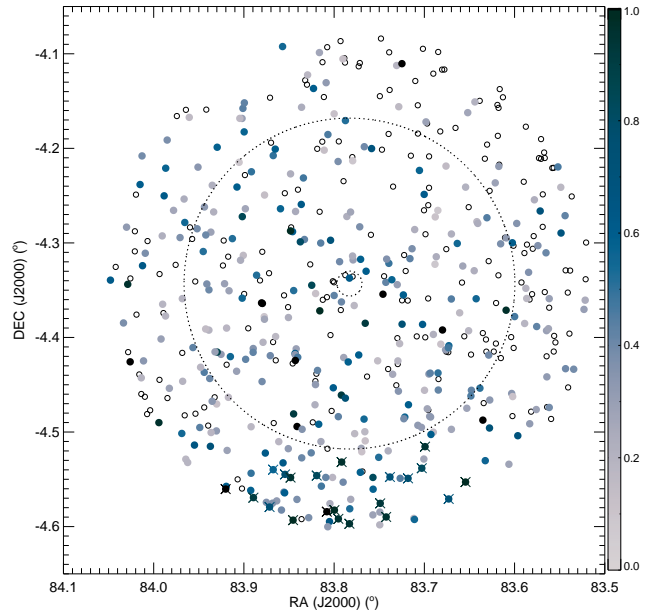


Figure 9. Sky chart comparing the removed field population (open circles) and remaining cluster stars (filled circles). Concentric circles represent the core radius and limiting radius respectively. Very reddened stars are marked with crosses. Colourbar indicates assigned membership probabilities.

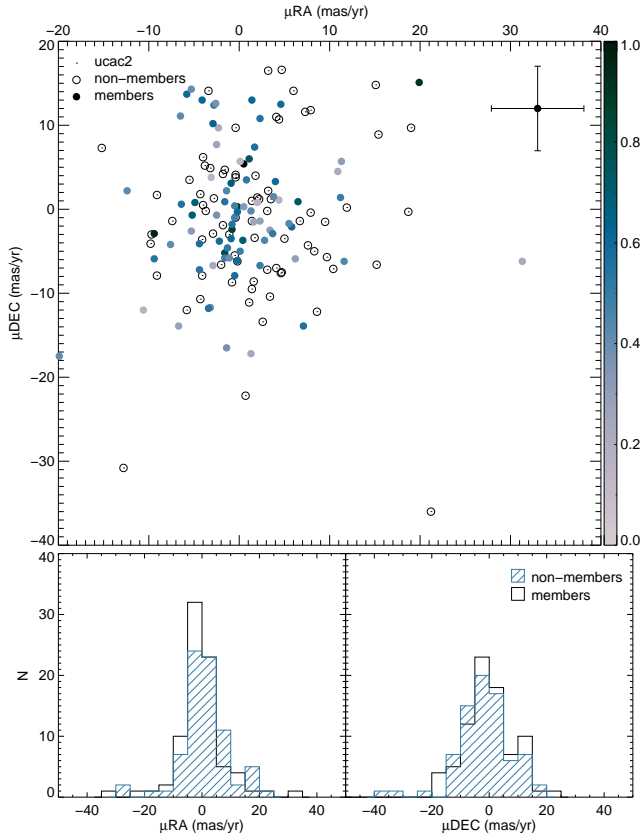


Figure 10. Correlation between our membership assignment and proper motion data taken from UCAC2 (top). Mean proper motion uncertainties are indicated. Probability distribution function of member and non-member stars are also shown in the bottom panels for RA (left) and DEC (right) proper motion directions.

5.3 Comparison with proper motion data

Proper motion data from UCAC2 (Zacharias et al. 2004) and UCAC3 (Zacharias et al. 2010) catalogues were used to investigate the reliability of the photometric memberships determined for the cluster stars. We selected stars within 15 arcmin from the cluster centre, with 2MASS photometry subject to the constraints described in Sect. 2.1 and only those with proper motions and their uncertainties. The corresponding samples amount to 159 objects in UCAC2 catalogue and 99 objects in UCAC3 catalogue.

Comparison of the UCAC2 proper motion with our membership results was done using the 2MASS designation to identify the common stars between the datasets. This allowed us to use our photometric membership to discriminate cluster and field-stars on the vector point diagram (VPD) (Fig. 10. top panel). Although the photometric members present a concentration near $(\mu\text{RA}, \mu\text{DEC}) = (0, 0)$, this is also true for the field stars, as can be more easily seen in the probability distribution histograms (bottom panels).

As the statistical distance between the cluster and field proper motion distributions is small, it is difficult to separate the populations. This effect becomes more accentuated for clusters where there is a large field to cluster member ratio or when the centroids of the proper motion distributions are very close to each other, such as in the case of NGC 1981. This problem has already been discussed

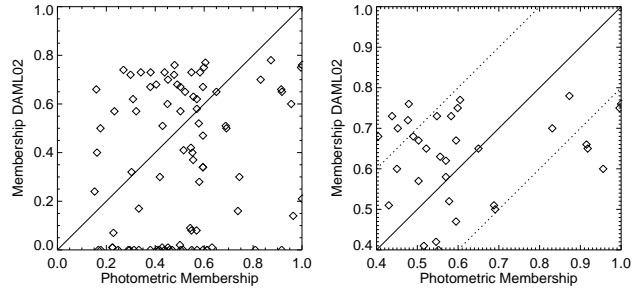


Figure 11. Correlation between the proper motion membership from DAML02 and our photometric memberships (left). Stars between the dotted lines have membership differences smaller than 20 per cent (right).

by Cabrera-Caño & Alfaro (1990) and Sánchez & Alfaro (2009) which proposed to use the spatial distribution of the stars, in addition to their proper motion distribution, to increase the statistical distance between the populations.

In fact, membership probabilities have been estimated for NGC 1981 by Dias et al. (2006) using UCAC2 proper motion of 160 stars within 15 arcmin of the cluster centre. The comparison between these memberships and the photometric memberships derived in this work shows a very poor correlation, as can be seen in Fig. 11 (left panel). Although the small statistical distance between the populations may account for the large scattering in the proper motion membership, especially for the low-membership stars, it seems that the derived photometric memberships are, in average, underestimated in relation to the proper motion ones. This trend is still visible when the low-membership stars are removed from both the photometric and proper motion sample, although the correspondence between the samples improves as most of the remaining stars present membership differences smaller than 20 per cent (right panel).

UCAC3 provided a complete new reduction of the Southern Proper Motion data that improved the proper motions of faint stars by a factor of 2 compared to UCAC2. Although this first release still presents some unsolved problems as described in Zacharias et al. (2010), we present a comparison of our results with proper motion from UCAC3 in Fig. 12. It is clear that UCAC3 VPD is sparser and less populated than that using UCAC2 data. However, it is currently not possible to realize the origin of this lack of stars (see Sect. 8 in Zacharias et al. 2010). Additionally, while our photometric analysis yields very entangled cluster and field populations in UCAC2 VPD, they are much better discriminated when proper motions from UCAC3 are considered (bottom panels of Fig. 10 and 12). Therefore, membership derived from UCAC3 proper motions might be in closer agreement with our photometric analysis.

6 ASTROPHYSICAL PARAMETERS

The optical data was correlated with the infrared data allowing the membership probabilities derived from 2MASS data to be assigned to the stars with *BVRi* photometry. Although shallower than the infrared sample and presenting larger photometric uncertainties, the optical data provided

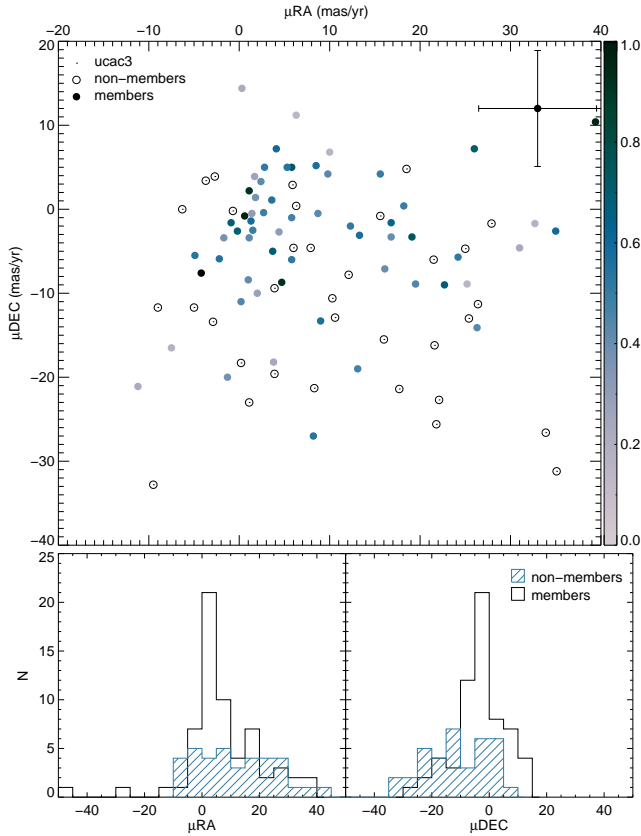


Figure 12. Similar to Fig. 10, but using UCAC3 proper motions.

a larger spectral base for the CMD analysis and additional constraints on the physical parameters.

Astrophysical parameters were determined by means of fittings of Padova isochrones for 2MASS (Bonatto et al. 2004) and Johnson-Cousins (Marigo et al. 2008) filters on the decontaminated CMDs. Pre-main sequence evolutionary tracks (Siess et al. 2000) were also employed. We chose only isochrones with overshooting and solar metallicity. As initial values for the cluster physical parameters we were guided by the previous studies of Kharchenko et al. (2005) and Bally (2008).

6.1 Age

The absence of evolved sequences in the CMDs due to the cluster youth makes determination of its age unreliable if one uses standard evolutionary models, i.e., those without accounting for pre-main sequence stars. Pre-main sequence isochrone fittings suggest that stars with ages ranging from 1-10 Myr coexists in the cluster and that most high-membership ($P > 0.6$) stars seems to fall between the young pre-main sequence isochrones of 1-5 Myr. This behaviour is also observed when only the innermost stars (inside the limiting radius) are considered. Fig. 8 shows the isochrone fittings on the decontaminated $J \times (J - H)$ and $J \times (J - K_s)$ CMDs along with the derived membership of stars. Fig. 13 shows the same fittings on the $V \times (V - I)$ and $V \times (V - J)$ CMDs. The average age derived for the cluster is 5 ± 1 Myr based on isochrone fittings to both near-infrared and optical data.

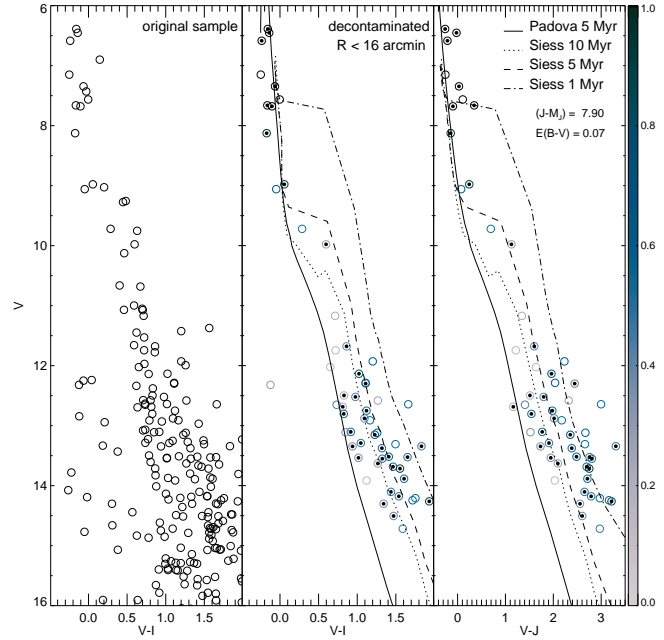


Figure 13. NGC 1981 decontaminated CMDs with optical data. Colours and symbols are the same as in Fig. 8.

In photometric studies of star clusters the MS turn-off is the most reliable feature for determining the age of these objects. However the identification of this CMD feature in very young clusters is uncertain by the scarcity of massive stars and the isochrones lack of turn-off sensitivity. For these objects the turn-on, the CMD locus where the PMS stars joins the MS, is a good indicator of the age of the stellar population.

From the isochrone fittings shown in Fig. 8 it can be seen that NGC 1981 turn-on is at $J \approx 9$, corresponding to an age of 5 Myr. Cignoni et al. (2010) devised a method to derive the age of young stellar systems by detecting the PMS turn-on with the luminosity function (LF). The clustering of stars at magnitudes near the turn-on produces a bump in the LF that becomes increasingly fainter as the cluster ages. By using synthetic simple stellar populations they calibrated a relation between the magnitude M_V of this luminosity bump and the age of the population.

The reddening and distance modulus determined in the present work were used to construct LFs with M_J and M_V for both the original and decontaminated sample, which are shown in Fig. 14. In both cases it was possible to identify a small bump in the LF at $M_J = 0.8 \pm 0.2$ and $M_V = 1.3 \pm 0.6$. This bump on the LF correspond to the age 3.3 ± 2.7 Myr, according to the age calibration with M_V by Cignoni et al. (2010).

However, as stated by Cignoni et al. (2010), reliable identification of the turn-on can only be made in populous clusters containing at least ≈ 50 stars brighter than $M_V = 5$ in order to successfully detect the bump among the Poissonian fluctuations. Therefore, although we should use this result with caution, it is in agreement, within the uncertainties, with the age and distance modulus obtained by means of isochrone fittings.

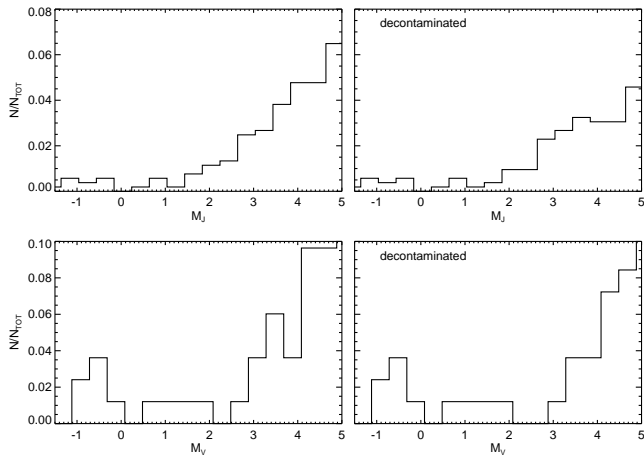


Figure 14. Luminosity functions in the infrared (top) and optical (bottom) bands. The turn-on bumps at $M_V=1.3$ and $M_J=0.8$ can be identified on both original (left) and decontaminated (right) samples.

6.2 Distance and Reddening

Although there were small discrepancies in the derived parameters (mainly on reddening) from optical versus infrared data, the mean determined values of distance modulus $J - M_J = 8.0 \pm 0.1$ and colour excess $E(B - V) = 0.07 \pm 0.03$ provided good isochrone fitting in both cases. With those values the true distance modulus is $(m - M)_0 = 7.9 \pm 0.1$ where we have used $A_J/A_V = 0.282$ and $A_V/E(B - V) = 3.09$ (Rieke & Lebofsky 1985), resulting in the distance of 380 ± 17 pc. The uncertainties were set to accommodate the values derived from the optimal fittings on both optical and infrared CMDs. These values are similar to the values found by Kharchenko et al. (2005). The almost 50 per cent deviation between optical and infrared reddening values deserves further discussion.

Although the literature reddening value provided a good isochrone fitting on the infrared data, the reddening value obtained from the $V \times (V - I)$ CMD suggests that the extinction in the optical bands is larger by a factor of 2.

Reddening in the optical bands was also determined in a previous work (Maia 2007) by a linear fit to the ZAMS (Schmidt-Kaler 1982) in colour-colour diagrams as proposed by Munari & Carraro (1996). By selecting the diagram most sensitive to reddening (Fig. 15) and limiting our analysis to stars brighter than $V = 13$ we derived a reddening value of $E(B - V) = 0.11$, which is very close to the value obtained from our best isochrone fitting on the optical data.

The reddening in the cluster direction, as interpolated in the dust maps by Schlegel et al. (1998), is $E(B - V) = 0.24 \pm 0.04$. Since these maps are sensitive to dust column density, this value can be considered as an upper limit to the cluster reddening. Also the cluster may be affected by differential reddening caused by the dust clouds in the region, specially for its southern part.

7 RADIAL MASS FUNCTION

To analyse the spatial dependence of the mass function (MF), the decontaminated LF in the J band determined

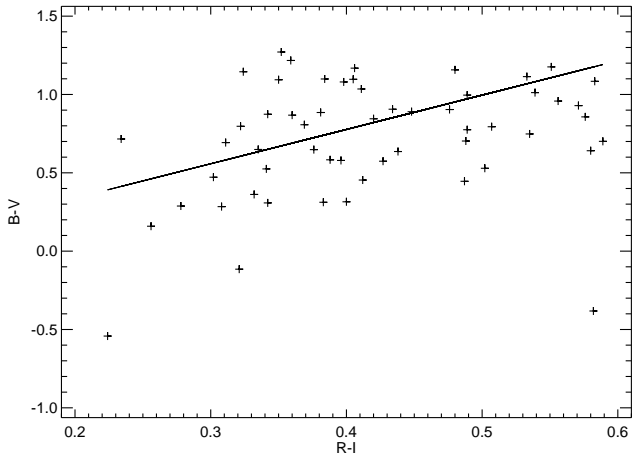


Figure 15. Colour-colour diagram with the optical data showing the ZAMS.

in Sect. 6.2 was used to investigate the regions comprehended within the inner 5.5 arcmin (half limiting radius) and within the range between 5.5 arcmin and the limiting radius (11 arcmin) of NGC 1981. The decontaminated LFs were converted into one MF for each region by fitting a mass-luminosity relation (in J band) from the combined PMS and evolved isochrones of 5 Myr at solar metallicity. The power law $\phi(m) = A \cdot m^{-(1+\chi)}$, where A is a normalization factor and χ is the MF slope, was fitted to the data in both regions. The MFs were normalized by the number of stars (N) inside each region ($N = 25$ for the inner region and $N = 81$ for the outer region). The outer region MF fit was limited to stars less massive than $\approx 1 M_\odot$ due to its small number of brighter stars. The MFs of the selected regions are presented in Fig. 16, together with the power-law fits and the determined slopes.

Both regions have MFs that are flatter than the Salpeter (1955) one, with slopes $\chi = 0.65 \pm 0.08$ (inner region) and $\chi = -0.44 \pm 0.03$ (outer region). Total mass inside each region was calculated by summing over selected mass ranges. We obtained for the inner region $m = 30 \pm 6 M_\odot$ ($0.4 < m(M_\odot) < 6$) and for the outer region $m = 107 \pm 13 M_\odot$ ($0.2 < m(M_\odot) < 9$). For the inner region the mass was also calculated by integrating the derived power law over the same mass range yielding $m = 38 \pm 2 M_\odot$. We should note that this mass implies an uniform distribution of stellar masses while the observed distribution of the brightest stars suffers from small number statistics.

The relaxation time of a star system can be defined as $t_{\text{relax}} = \frac{N}{8 \ln N} t_{\text{cross}}$, where $t_{\text{cross}} = R/\sigma_v$ is the crossing time, N is the total number of stars and σ_v is the velocity dispersion (Binney & Tremaine 1987; Lada & Lada 2003). By using the dispersion in proper motion given by DAML02 for 31 stars within 11 arcmin from the cluster centre with membership probability (derived by DAML02) above 50 per cent and assuming an isotropic distribution of spatial velocities we estimated a mean velocity dispersion $\sigma_v \approx 8 \text{ km.s}^{-1}$. Combining this information with the limiting radius we get $t_{\text{cross}} = R/\sigma_v = 0.15 \text{ Myr}$ and $t_{\text{relax}} = 0.41 \text{ Myr}$ for $N = 106$ stars.

Although unexpected for such a young object, dynamical evolution can be responsible for rapid collapse of the clus-

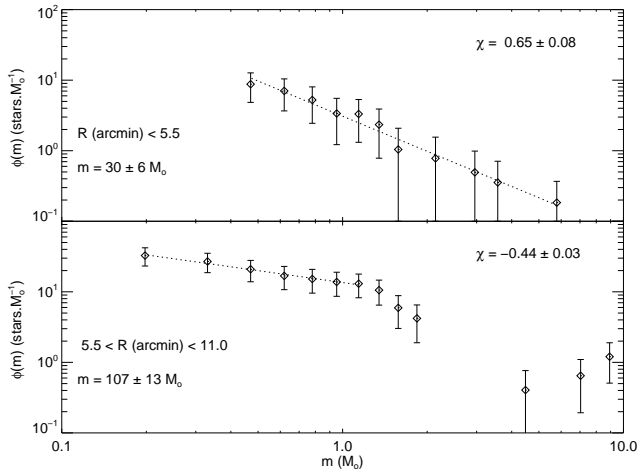


Figure 16. Mass function of stars inside the inner 5.5 arcmin (top) and within the range 5.5-11 arcmin (bottom). Power law fittings, resulting slopes and total mass are indicated. Error bars correspond to 1- σ fluctuations

ter core causing mass segregation and evaporation of stars in outer regions. This may have occurred in NGC 1981 since the relaxation time of the cluster is much smaller than its age. As shown in Fig. 16 the mass function slope is larger for the inner 5.5 arcmin than for the outer 5.5-11 arcmin annular region between the mass range 0.4-1.1 M_{\odot} . This is in apparent contradiction with the expected consequences of dynamical evolution, i.e., the existence of an excess of low mass stars and depletion of massive ones (eventually grouped in binaries and/or multiple systems) in the outer region compared to the inner region. However we indeed do not found any star with mass lower than 0.4 M_{\odot} in the inner region but 23 stars in the same mass range in the outer region, in agreement with the mass segregation scenario.

8 STAR DENSITY MAPS

We have mapped the projected spatial star density and the frequency of stars in different positions of the CMD (Hess diagram). Firstly we show in Fig. 17 the star density map and the corresponding Hess diagram of a large region around NGC 1981 including the Orion Nebula Cluster (ONC). Both diagrams were built by dividing the plots in square cells of 32 pixels on a side, which in Fig. 17 corresponds to 5.6 arcmin for the spatial map, 0.1 in $(J - K_s)$ and 0.4 mag in J for the Hess diagram. The density diagrams are then smoothed by a cubic convolution interpolation method.

The data comprises all sources extracted from 2MASS catalogue obeying the photometric quality constraints mentioned in Sect. 2.1. The ONC dominates the density map southwards of NGC 1981 which the centre, as determined in Sect. 3, is indicated by a square. Even though, an over-density compared to the adjacent neighbourhood can be noticed at the position of NGC 1981. The Hess diagram provide evidence that most of the stellar content in the ONC consists of red low mass stars.

Smaller sky and CMD areas were considered around NGC 1981 in Fig. 18. The square cells of 32 pixels correspond to 2.4 arcmin for the spatial map and 0.02 in $(J - K_s)$,

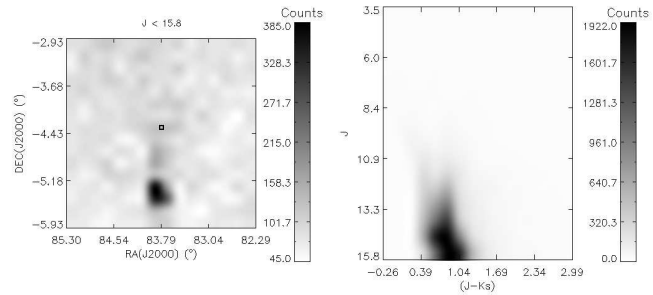


Figure 17. Star density map (left) and Hess diagram (right) of a region $3^{\circ} \times 3^{\circ}$ centred in NGC 1981 (square) based on 2MASS data.

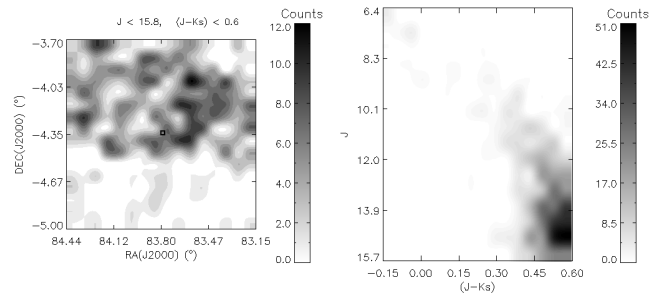


Figure 18. Same as Fig. 17 but for a smaller region centred in NGC 1981 and $(J - K_s) < 0.6$.

0.3 mag in J for the Hess diagram. The spatial map has $1.3^{\circ} \times 1.3^{\circ}$ and the associated Hess diagram has been limited to contain only stars with $(J - K_s) < 0.6$, thus excluding the reddest stars. Such a colour constraint clearly separates the spatial map in two regions: a denser star field northwards of NGC 1981 (but including it) and a more rarefied star field southwards of NGC 1981. It clearly reflects the presence of dust revealing a boundary between a heavy obscured stellar field and a region with lower extinction. It also indicates where the reddest stellar population lies in the area. The cut in colour eliminates reddened stars by dust but also pre-main sequence stars, known to be abundant in the ONC region.

Fig. 19 shows the spatial stellar density plots for the same area as in Fig. 18, but with progressive cuts in star brightness, allowing one to connect the density peaks with different populations characterized by a limit magnitude. The plots show the emergence of NGC 1981 as the limiting magnitude varies from $J = 15.8$ to 10.

Although NGC 1981 is in a region of intense star formation with clouds of dust and gas, it has presently inhabited a relatively dust-free field, perhaps as a consequence of the cluster evolution. Its massive stellar content may have contributed to the energy release into the interstellar medium, either by means of exploding supernovae and/or winds due to radiation pressure. Our study concludes that NGC 1981 is a cluster older than the ONC and NGC 1977, which are still embedded in the parental gas and dust cloud, and that its structure is best visualized by considering stars brighter than $J = 12$.

Fig. 20 shows the same analysis applied to probable

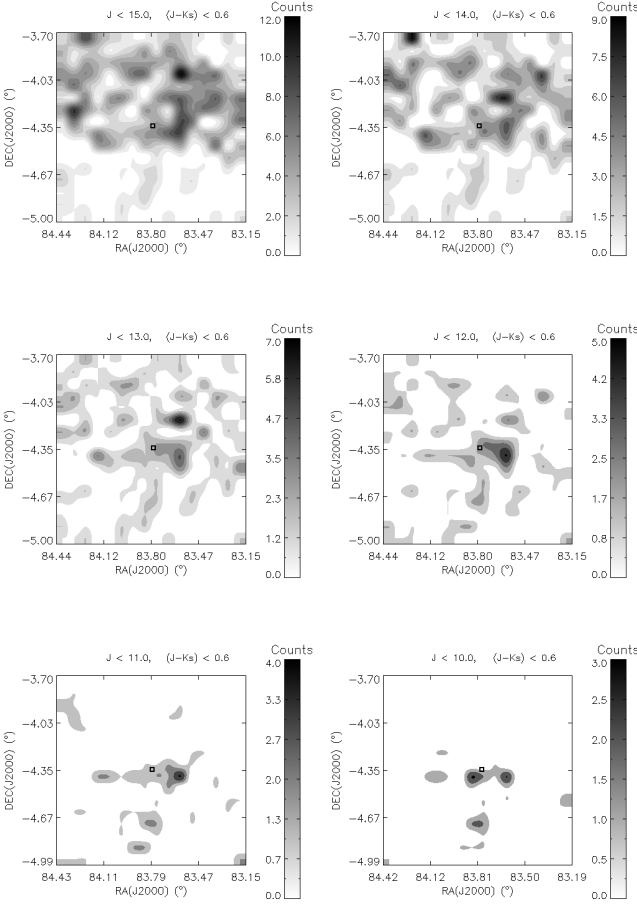


Figure 19. Star density maps for $(J - K_s) < 0.6$ and variable J magnitude limit as indicated.

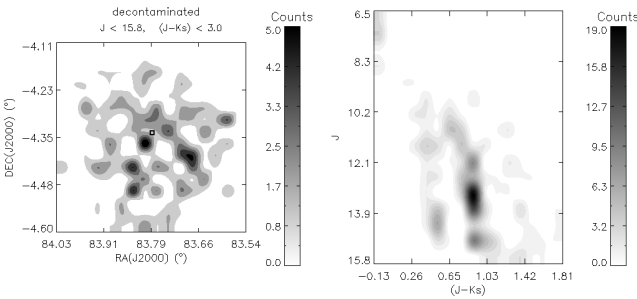


Figure 20. Decontaminated star density map (left) and Hess diagram (right) for a circular region of $R = 15$ arcmin centred in NGC 1981.

members inside a circle of radius $R = 15$ arcmin centred in the cluster. As a consequence of the method applied for field decontamination, the cluster stellar content is more clearly defined down to the photometric limit of the data. The underlying stellar field and the cluster stellar population were indistinguishable in the previous contaminated diagrams for stars fainter than $J = 12$ (Figs. 17 to 19). In Fig. 20, a population of pre-main sequence members stands out in the Hess diagram.

9 DISCUSSION AND CONCLUSIONS

We investigated the stellar object NGC 1981, a young star cluster in the Gould's Belt nearby the Orion Nebula Cluster containing a small population of massive B type stars. We employed near-infrared data from 2MASS to calculate the cluster centre at $\alpha = 5^{\text{h}}35^{\text{m}}08^{\text{s}}$, $\delta = -04^{\circ}20'35''$ and to subsequently derive the structural parameters from King-profile fittings obtaining a core radius $R_c = 0.09 \pm 0.04$ pc and central density $\sigma_0 = (2 \pm 1) \times 10^2 \text{ stars.pc}^{-2}$. A limiting radius of $R_{\text{lim}} = 1.21 \pm 0.11$ pc was also derived from the radial density profile.

We devised a decontamination procedure based on the method by Bonatto & Bica (2007) to statistically remove the underlying field population from the cluster CMD by using an offset-field to sample the background contamination. Tested on NGC 1981 with multiple offset-fields, the procedure reliably presented an average field-star exclusion efficiency of 84 per cent, separating cluster members with an average deviation of 5 per cent in the number of stars. It also provides photometric membership for the member stars with average uncertainty of 6 per cent, depending on the selection of the offset-field.

By using optical $BV(RI)_C$ data alongside 2MASS data we performed isochrone fittings on the decontaminated data and determined average values of reddening $E(B - V) = 0.07 \pm 0.03$, distance modulus $(m - M) = 7.9 \pm 0.1$ ($d = 380 \pm 17$ pc) and age 5 ± 1 Myr. The relation between the turn-on M_V and age (Cignoni et al. 2010) was also used as an additional check for the cluster age. In this case the age derived was 3.3 ± 2.7 Myr. The scarcity of bright stars make this value unreliable as sole indicator of age. We use it to infer that the luminosity of the turn-on is consistent with the age and distance modulus found by isochrone fittings.

By comparing our derived memberships with proper motions from UCAC2 catalogue, we showed that while the small statistical distance between cluster and field populations may have hardened their separation in the VPD, the photometric method was capable to discern these very entangled populations. Indeed, by comparing our derived memberships with proper motions from UCAC3, we were able to distinguish a clear concentration of member stars over a sparse distribution of non-member stars in the VPD.

We derived mass functions for stars inside the inner 5.5 arcmin and 11 arcmin (limiting radius) and evaluated the total mass inside these regions: $m = 30 \pm 6 M_{\odot}$ and $m = 107 \pm 13 M_{\odot}$, respectively. After fitting a power law to the data, the calculated slopes $\chi = 0.65 \pm 0.08$ (inner region) and $\chi = -0.44 \pm 0.03$ (outer region) are flatter than the Salpeter MF, indicating a depletion of low mass stars in the outer region relative to the inner region. Cluster evolution and mass segregation can explain this effect if the cluster has had time to dynamically evolve. In fact, by using proper motion data from DALM02 for stars inside the limiting radius we have derived $t_{\text{cross}} = 0.15$ Myr and $t_{\text{relax}} = 0.41$ Myr, meaning that the cluster stars had time to interact gravitationally with each other forming binaries and/or multiple systems composed by massive stars that settle in the cluster centre and leading to the ejection of low mass stars towards the cluster outer regions.

The cluster might have undergone mass loss in the earlier stages of the star forming process leading to the present

sparse structure. The energy released into the medium by the evolution of the most massive stars (i.e. by supernovae and stellar winds) may have cleared the cluster from its parental cloud of gas and dust causing a collapse of the core due to the changing gravitational potential and subsequent evaporation of stars in its outer regions.

Through stellar density maps we discriminated the presence of a embedded red population of stars just south of NGC 1981. These stars are likely members of the young object NGC 1977 and still contaminate the southern population of NGC 1981. These maps also demonstrate the power of the procedure employed to disentangle field-stars from the cluster population.

As the majority of young open clusters, NGC 1981 is not expected to live longer than a few Myr, evolving from its actual state of marginally bound system to a loose stellar association and finally dispersing itself into the Galactic disc.

ACKNOWLEDGMENTS

We thank the referee, G. Carraro, for helping to improve this paper. We also thank C. Bonatto for the insightful comments that helped to develop this work. We thank the Brazilian financial agencies FAPEMIG (grants APQ00154/08, APQ00117/08) and CNPq. We also thank the OPD staff for their support at the observatory. This publication makes use of data products from the Two Micron All Sky Survey, which is a joint project of the University of Massachusetts and the Infrared Processing and Analysis Center/California Institute of Technology, funded by the National Aeronautics and Space Administration and the National Science Foundation. This research has made use of the WEBDA database, operated at the Institute for Astronomy of the University of Vienna, and of the SIMBAD database, operated at CDS, Strasbourg, France. This research has made use of Aladin.

REFERENCES

- Bally J., 2008, in Bo Reipurth, ed., ASP Monograph 4, Handbook of Star Forming Regions, Vol I: The Northern Sky, p. 459
- Binney J., Tremaine S., 1987, Galactic Dynamics, Princeton University Press, Princeton, NJ
- Bonatto C., Bica E. Girardi L., 2004, A&A, 415, 571
- Bonatto C., Santos Jr. J.F.C., Bica E., 2006, A&A, 445, 567
- Bonatto C., Bica E., 2007, MNRAS, 377, 1301
- Cabrera-Caño J., Alfaro E. J., 1990, A&A, 235, 94
- Cignoni M., Tosi M., Sabbi E., Nota A., Degl’Innocenti S., Prada Moroni P.G., Gallagher J.S., 2010, ApJ, 712, L63
- D’Antona F., 2002, IAUS, 207, 599
- Dias W.S., Alessi B.S., Moitinho A., Lepine J.R.D., 2002, A&A, 389, 871
- Dias W.S., Assafin M., Flório V., Alessi B.S., LÍbero V., 2006, A&A, 446, 949
- Elias F., Alfaro E.J., Cabrera-Caño J., 2009, MNRAS, 397, 2
- Hron J., 1987, A&A, 176, 34
- Jacobson H.R., Pilachowski C.A., Friel E.D., 2008, in J.G. Funes, E.M. Corsini, eds, ASP Conf. Ser. Vol 396, Formation and Evolution of Galaxy Disks, p. 73
- Kharchenko N.V., Piskunov A.E., Röser S., Schilbach E., Scholz R.D., 2005, A&A, 438, 1163
- King I., 1962, AJ, 67, 471
- Lada C.J., Lada E.A., 2003, ARA&A, 41, 57
- Landin N.R., Ventura P., D’Antona F., Mendes L.T.S., Vaz L.P.R., 2006, A&A, 456, 269
- Landolt A.U., 1992, AJ, 104, 340
- Lesh J.R., 1968, ApJS, 17, 371
- Maia F.F.S., 2007, Master Dissertation, UFMG
- Marigo P., Girardi L., Bressan A., Groenewegen M.A.T., Silva L., Granato G.L., 2008, A&A, 482, 883
- Muench A., Getman K., Hillenbrand L., Preibisch T. 2008, in Bo Reipurth, ed., ASP Monograph 4, Handbook of Star Forming Regions, Vol I: The Northern Sky, p. 483
- Munari U., Carraro G., 1996, A&A, 314, 108
- Pavani D.B., Bica, E., 2007, A&A, 468, 139
- Piatti A.E., Clariá J.J., Abadi M.G., 1995, AJ, 110, 2813
- Piskunov A.E., Kharchenko N.V., Rser S., Schilbach E., Scholz R.D., 2006, A&A, 445, 545
- Pöppel, W.G.L. 2001, in T. Montmerle & P. André, eds, ASP Conf. Ser. Vol 243, From Darkness to Light: Origin and Evolution of Young Stellar Clusters, Astron. Soc. Pac., San Francisco, p. 667
- Rieke G.H., Lebofsky M.J., 1985, ApJ, 288, 618
- Sánchez N., Alfaro E. J., 2009, ApJ, 696, 2086
- Salpeter E., 1955, ApJ, 121, 161
- Santos Jr. J.F.C., Bonatto C., Bica E., 2005, A&A, 442, 201
- Schlegel D.J., Finkbeiner D.P., Davis M., 1998, ApJ, 500, 525
- Schmidt-Kaler Th., 1982, in Landolt-Bornstein New Series Vol. 2b: Astronomy and Astrophysics/Star and Star clusters. Springer-Verlag, Newbak, p. 14
- Sestito P., Bragaglia A., Randich S., Pallavicini R., Andrievsky S.M., Korotin S.A., 2008, A&A, 488, 943
- Sharpless S., 1952, ApJ, 116, 251
- Siess L., Dufour E., Forestini M., 2000, A&A, 358, 593
- Skrutskie M.F., Cutri R.M., Stiening R., et al., 2006, AJ, 131, 1163
- Subramaniam A., Gorti U., Sagar R., Bhatt H.C., 1995, A&A, 302, 86
- Zacharias N., Urban S. E., Zacharias M. I., Wycoff G. L., Hall D. M., Monet D. G., Rafferty T. J., 2004, AJ, 127, 3043
- Zacharias N., et al., 2010, AJ, 139, 2184